THREE DIMENSIONAL CODE VALIDATION FOR TRANSITION PHENOMENA

Leandro F. de Souza
Instituto Tecnológico de Aeronáutica
Pç Mal. Eduardo Gomes, 50 - São José dos Campos, SP - 12228 900, Brazil
lefraso@zipmail.com.br

Márcio T. Mendonça
Centro Técnico Aeroespacial, Instituto de Aeronáutica e Espaço
Pç Mal. Eduardo Gomes, 50 - São José dos Campos, SP - 12228 904, Brazil
marcio_tm@yahoo.com

Marcello A. Faraco de Medeiros
USP - Universidade de São Paulo
Escola de Engenharia de São Carlos - Departamento de Engenharia Aeronáutica
Av. Trabalhador São Carlense, 400 - SP - 13566-590, Brazil
marcello@sc.usp.br

Markus Kloker
Institut für Aerodynamik und Gasdynamik - Universität Stuttgart
Stuttgart, Germany
mkloker@iag.uni-stuttgart.de

Abstract. *A three-dimensional numerical method for solving the complete Navier-Stokes equations for incompressible flows in a flat plate is presented. The governing equations are written in vorticity-velocity formulation. The Method is a combination of a compact 6th order spatial approximations in the normal direction and streamwise directions and a Fourier spectral approximations in the spanwise direction. A 4th order Runge-Kutta method is used for integration in time and a Multi-grid technique is used to accelerate the convergence of the Poisson solver. The disturbances are introduced at the wall via a suction and blowing strip. The code is first validated by comparing results with Linear Stability Theory, in which small amplitude disturbances propagate in the flow field. In order to investigate the non linear behavior, results for fundamental and subharmonic resonances are presented and compared with results obtained experimentally and numerically with a Parabolized Stability Equation code. The comparisons show that the proposed method can accurately calculate the propagation of Tollmien-Schlichting type disturbances in a flat plate. The code is then used to investigate the instability of a boundary layer when both subharmonic and fundamental modes are present simultaneously.*

Key words: *Direct numerical simulation, hydrodynamic stability, compact difference schemes, high order finite-differences, fundamental and subharmonic resonance*

1. Introduction

In general, turbulent flows are the most common in practical applications. Nevertheless, there are a large number of situations in which transition to turbulence is of significant importance. For example, in the flow over low Reynolds number turbine blades and laminar flow airfoils. The understanding of how transition takes place can help in predicting and even controlling transition to turbulence. Over recent years the body of knowledge on laminar flow stability and transition has increased dramatically due to the development of new experimental and numerical techniques as well as due to advances in applied mathematical theories. Nevertheless, there are many transition scenarios for which a physical explanation is still unknown, and predicting transition location is still a challenge in many engineering applications

This work is part of an ongoing project that aims at developing numerical methods suitable for the investigation of laminar flow stability problems. The fast advancements in computer technology is making direct numerical simulations a reality. In the late 70´s a few works were already targeting instability problems with numerical simulations (Fasel, 1976), but mostly using temporal approximations. The 80´s saw the development of more advanced approaches on numerical techniques (Wray and Hussaini, 1994; Rai and Moin, 1989; Laurien and Kleiser, 1989; Herbert, 1991), but only in the 90´s these techniques did show there full potential due to the developments in hardware (Moin and Mahesh, 1998; Meitz and Fasel, 2000). Today there is a strong push to apply high order techniques to increasingly complex problems (Carpenter et al., 2002).

In this paper a numerical technique for the solution of incompressible instability problems is presented (Section 2). The method is based on a compact high order finite differences scheme (Souza et al., 2001;

Lele, 1992; Kloker, 1998). The computer code is verified against linear stability theory and experimental and numerical nonlinear results (Section 3). Having done that the code is used to investigate the behavior of two classic instability modes, namely, fundamental and subharmonic resonances, when more than one mode is active (Section 4). A similar study has been presented recently (Mendonça and Medeiros, 2000) and the general conclusion was that when both fundamental and subharmonic resonances are active the subharmonic mode is predominant. That study is extended to situations where the different stability modes do not have similar initial strengthes.

2. Formulation and Numerical Method

2.1. Governing Equations

In this study, the governing equations are the incompressible, unsteady Navier-Stokes equations with constant density and viscosity. They consist of momentum equations for the velocity components in the streamwise direction (x), wall normal direction (y) and in the spanwise direction (z):

$$\frac{\partial u_x}{\partial t} + u_x\frac{\partial u_x}{\partial x} + u_y\frac{\partial u_x}{\partial y} + u_z\frac{\partial u_x}{\partial z} = -\frac{\partial p}{\partial x} + \nabla^2 u_x, \tag{1}$$

$$\frac{\partial u_y}{\partial t} + u_x\frac{\partial u_y}{\partial x} + u_y\frac{\partial u_y}{\partial y} + u_z\frac{\partial u_y}{\partial z} = -Re\frac{\partial p}{\partial y} + \nabla^2 u_y, \tag{2}$$

$$\frac{\partial u_z}{\partial t} + u_x\frac{\partial u_z}{\partial x} + u_y\frac{\partial u_z}{\partial y} + u_z\frac{\partial u_z}{\partial z} = -\frac{\partial p}{\partial z} + \nabla^2 u_z, \tag{3}$$

and the continuity equation:

$$\frac{\partial u_x}{\partial x} + \frac{\partial u_y}{\partial y} + \frac{\partial u_z}{\partial z} = 0, \tag{4}$$

where p is the pressure, Re is the Reynolds number and $\nabla^2$is:

$$\nabla^2 = \frac{1}{Re}\frac{\partial^2}{\partial x^2} + \frac{\partial^2}{\partial y^2} + \frac{1}{Re}\frac{\partial^2}{\partial z^2}. \tag{5}$$

The variables used in the above equations are non dimensional. They were related to the dimensional variables by:

$$x = \frac{\bar{x}}{\bar{L}}, \quad y = \frac{\bar{y}}{\bar{L}}\sqrt{Re}, \quad z = \frac{\bar{z}}{\bar{L}}, \quad u_x = \frac{\bar{u_x}}{\bar{U_\infty}}, \quad u_y = \frac{\bar{u_y}}{\bar{U_\infty}}\sqrt{Re}, \quad u_z = \frac{\bar{u_z}}{\bar{U_\infty}}, \quad Re = \frac{\bar{U_\infty}\bar{L}}{\bar{\nu}} \tag{6}$$

where over-bar were used in dimensional terms. $\bar{L}$ is the reference length, $\bar{U_\infty}$ is the free-stream velocity and $\bar{\nu}$ is the kinematic viscosity.

The vorticity components, given by the negative curl of the velocity are:

$$\omega_x = \frac{1}{Re}\frac{\partial u_y}{\partial z} - \frac{\partial u_z}{\partial y}, \qquad \omega_y = \frac{\partial u_z}{\partial x} - \frac{\partial u_x}{\partial z}, \qquad \omega_z = \frac{\partial u_x}{\partial y} - \frac{1}{Re}\frac{\partial u_y}{\partial x}, \tag{7}$$

Taking the curl of the momentum equations (1 to 3) and using the fact that both the velocity and the vorticity vectors are solenoidal, one can obtain the vorticity transport equation in each direction:

$$\frac{\partial \omega_x}{\partial t} + \frac{\partial a}{\partial y} - \frac{\partial b}{\partial z} = \nabla^2\omega_x, \tag{8}$$

$$\frac{\partial \omega_y}{\partial t} + \frac{\partial c}{\partial z} - \frac{\partial a}{\partial x} = \nabla^2\omega_y, \tag{9}$$

$$\frac{\partial \omega_z}{\partial t} + \frac{\partial b}{\partial x} - \frac{\partial c}{\partial y} = \nabla^2\omega_z, \tag{10}$$

where:

$$a = u_y\omega_x - u_x\omega_y, \qquad b = u_x\omega_z - u_z\omega_x \qquad \text{and} \qquad c = u_z\omega_y - u_y\omega_z, \tag{11}$$

are the nonlinear terms resulting from convection and vortex stretching.

Taking the definition of the vorticity and again using the fact that both velocity and vorticity vectors are solenoidal, one can obtain a Poisson equation for each velocity component:

$$\frac{\partial^2 u_x}{\partial x^2} + \frac{\partial^2 u_x}{\partial z^2} = -\frac{\partial \omega_y}{\partial z} - \frac{\partial^2 u_y}{\partial x \partial y}, \tag{12}$$

$$\frac{1}{Re}\frac{\partial^2 u_y}{\partial x^2} + \frac{\partial^2 u_y}{\partial y^2} + \frac{1}{Re}\frac{\partial^2 u_y}{\partial z^2} = -\frac{\partial \omega_z}{\partial x} + \frac{\partial \omega_x}{\partial z}, \tag{13}$$

$$\frac{\partial^2 u_z}{\partial x^2} + \frac{\partial^2 u_z}{\partial z^2} = \frac{\partial \omega_y}{\partial x} - \frac{\partial^2 u_y}{\partial y \partial z}. \tag{14}$$

In the calculations presented here, the flow was assumed to be periodic and symmetric with respect to $Z = 0$ in the spanwise (z) direction. Taking this assumptions, the flow field was expanded in a real Fourier cosine and sine series with K spanwise Fourier modes:

$$(u_x, u_y, \omega_z, b, c) = \sum_{k=0}^{K} (U_{x_k}, U_{y_k}, \Omega_{z_k}, B_k, C_k) \cos(\beta_k z), \tag{15}$$

$$(u_z, \omega_x, \omega_y, a) = \sum_{k=1}^{K} (U_{z_k}, \Omega_{x_k}, \Omega_{y_k}, A_k) \sin(\beta_k z), \tag{16}$$

where β_k is the spanwise wavenumber given by $\beta_k = (2\pi k)/\lambda_z$, and λ_z is the spanwise wavelength of the lowest spanwise Fourier mode.

Substituting the sine and cosine transforms Eq. (15) and (16) in the vorticity transport equations (8) to (10) and in the velocity Poisson equations (12) to (14), yields the governing equations in the Fourier space:

$$\frac{\partial \Omega_{x_k}}{\partial t} + \frac{\partial A_k}{\partial y} - \beta_k B_k = \nabla_k^2 \Omega_x, \tag{17}$$

$$\frac{\partial \Omega_{y_k}}{\partial t} + \beta_k C_k - \frac{\partial A_k}{\partial x} = \nabla_k^2 \Omega_y, \tag{18}$$

$$\frac{\partial \Omega_{z_k}}{\partial t} + \frac{\partial B_k}{\partial x} + \frac{\partial C_k}{\partial y} = \nabla_k^2 \Omega_z, \tag{19}$$

$$\frac{\partial^2 U_{x_k}}{\partial x^2} - \beta_k^2 U_{x_k} = -\beta_k \Omega_{y_k} - \frac{\partial^2 U_{y_k}}{\partial x \partial y}, \tag{20}$$

$$\frac{1}{Re}\frac{\partial^2 U_{y_k}}{\partial x^2} + \frac{\partial^2 U_{y_k}}{\partial y^2} - \beta_k^2 U_{y_k} = -\frac{\partial \Omega_{z_k}}{\partial x} + \beta_k \Omega_{x_k}, \tag{21}$$

$$\frac{\partial^2 U_{z_k}}{\partial x^2} - \beta_k^2 U_{z_k} = \frac{\partial \Omega_{y_k}}{\partial x} + \beta_k \frac{\partial U_{y_k}}{\partial y}. \tag{22}$$

where ∇_k^2 is:

$$\nabla_k^2 = \frac{1}{Re}\frac{\partial^2}{\partial x^2} + \frac{\partial^2}{\partial y^2} - \beta_k^2, \tag{23}$$

2.2. Numerical Model

The equations (17) to (22) were solved numerically inside a rectangular integration domain. The integration domain is shown schematically in Fig.(1). The fluid enters the computational domain in $x = x_0$ and exits at the outflow boundary $x = x_{max}$. Disturbances were introduced into the flow field using a periodical suction and blowing function at the wall in a disturbance strip. This region is located between x_1 and x_2. Before the introduction of disturbances in the flow field, a 2D boundary layer was simulated to avoid numerical disturbances associated with the use of a Blasius solution. The values for the u_x, u_y and ω_z obtained from this 2D simulation were used as the base flow. In the region located between x_3 and x_4 a buffer domain technique was implemented in order to avoid wave reflections at the outflow boundary.

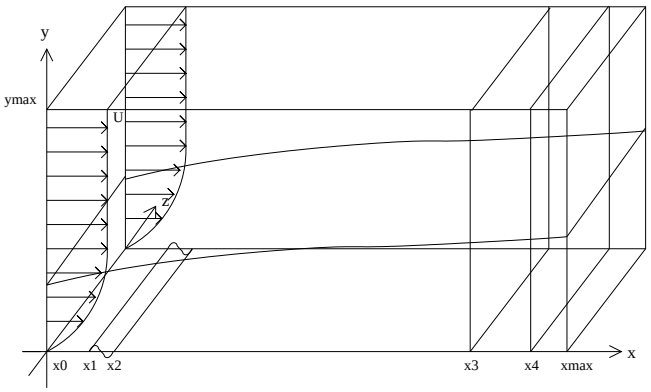

Figure 1: Integration domain.

Boundary conditions:

At the inflow boundary ($x = x_0$), all velocity and vorticity components were specified.

At the outflow boundary ($x = x_{max}$), the second derivative of the velocity and vorticity components were setted to zero:

$$\frac{\partial^2 F_k}{\partial x^2} = 0, \tag{24}$$

where $F_k = \{U_{x_k}, U_{y_k}, U_{z_k}, \Omega_{x_k}, \Omega_{y_k}, \Omega_{z_k}\}$.

At the upper boundary $y = y_{max}$ the flow was assumed to be irrotational. This was satisfied setting all vorticity and their derivatives to zero. An exponential decay of the velocity was imposed using the condition:

$$\frac{\partial U_{y_k}}{\partial y}|_{x,y_{max},t} = -\frac{\alpha^*}{\sqrt{Re}} U_{y_k}(x, y_{max}, t), \tag{25}$$

where $\alpha^* = \sqrt{\alpha^2 + \beta_k^2}$ and α is the local expected wavenumber.

At the wall ($y = 0$), no-slip conditions were imposed for the streamwise (U_{x_k}) and the spanwise (U_{z_k}) velocity components. For the wall normal velocity component (U_{y_k}) the non-slip conditions were imposed in all points at the wall except between $x1$ and $x2$, where the disturbances were introduced. In addition the condition $\partial U_{y_k}/\partial y = 0$ was imposed to ensure conservation of mass. The following equations were used for evaluating the vorticity components at the wall:

$$\frac{\partial^2 \Omega_{x_k}}{\partial x^2} - \beta_k^2 \Omega_{x_k} = -\frac{\partial^2 \Omega_{y_k}}{\partial x \partial y} - \beta_k (\nabla_k^2 V_k), \tag{26}$$

$$\frac{\partial \Omega_z}{\partial x} = \beta_k \Omega_{x_k} - \nabla_k^2 V_k. \tag{27}$$

The introduction of the disturbances at the wall, according to Fasel et al., 1990, has proved to be a very efficient way of introducing Tollmien-Schlichting (TS) waves in the flow field. The method consist of introducing a slot at the wall ($i_1 \leq i \leq i_2$), where i_1 and i_2 are,respectively, the first and the last point of the disturbance strip, in x direction. The function used for the normal velocity U_{y_k} was:

$$\begin{aligned} U_{y_k}(i, 0, t) &= f_1(\epsilon) A \sqrt{Re} \sin(\omega_t t + \theta) \qquad \text{for} \qquad i_1 \leq i \leq i_2 \\ &\qquad\qquad\qquad\qquad\qquad\qquad\qquad\qquad\qquad\qquad \text{and} \\ U_{y_k}(x, 0, t) &= 0 \qquad \text{for} \qquad i < i_1 \quad \text{and} \quad i > i_2. \end{aligned} \tag{28}$$

The values of A and θ are real constants that can be chosen to adjust the amplitude and phase of the blowing and suction disturbances. The constant ω_t is the dimensionless frequency. The function $f_1(\epsilon)$ adopted was a fifth order function, proposed by Zhang and Fasel, 1999. This function is used in order to make sure that, at $y = 0$, the vertical velocity component, its first and second derivatives do not have a discontinuity going in and out of the suction and blowing region. The function is:

$$
\begin{aligned}
f_1(\epsilon) &= \frac{1}{48}(729\epsilon^5 - 1701\epsilon^4 + 972\epsilon^3) \qquad \text{if} \qquad i_1 \leq i \leq \frac{1}{2}(i_1 + i_2) \\
\text{where} \qquad & \epsilon = 2\frac{i - i_1}{i_2 - i_1} \\
& \\
f_1(x) &= \frac{-1}{48}(729\epsilon^5 - 1701\epsilon^4 + 972\epsilon^3) \qquad \text{if} \qquad \frac{1}{2}(i_1 + i_2) \leq i \leq i_2 \\
\text{where} \qquad & \epsilon = 2\frac{i_2 - i}{i_2 - i_1}
\end{aligned}
\tag{29}
$$

The variable i indicates the grid point location x_i in the streamwise direction, and points i_1 and i_2 correspond to x_1 and x_2 respectively.

The shape of the function $f_1(\epsilon)$ and its second derivative at the blowing and suction region are plotted in Figs.(2) and (3).

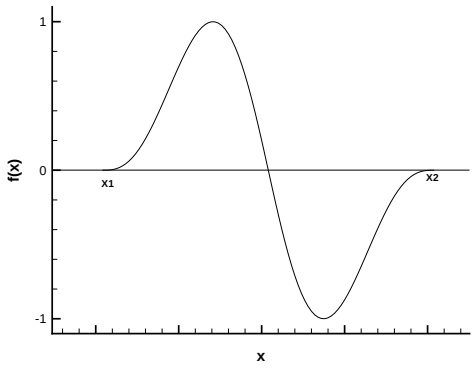

Figure 2: Normal velocity distribution at the suction and blowing region.

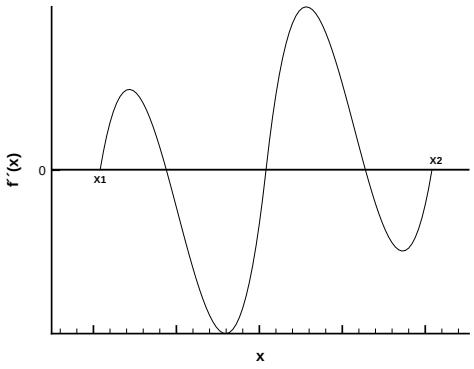

Figure 3: Second derivative of the normal velocity distribution at the suction and blowing region.

A damping zone near the outflow boundary was defined in which all the disturbances were gradually damped down to zero. This technique is well documented in Kloker et al., 1993, where the advantages and requirements are discussed. Meitz and Fasel, 2000 adopted a fifth order polynomium in their work, and the same function was used in the present simulations. The basic idea is to multiply the vorticity components by a ramp function $f_2(x)$ after each step of the integration method. This technique has proved to be very efficient in avoiding reflections that could come from the outflow boundary conditions when simulating disturbed flows. Using this technique, the vorticity components were taken as:

$$\Omega_k(x, y) = f_2(x)\Omega_k(x, y, t), \tag{30}$$

where $\Omega_k(x, y, t)$ is the disturbance vorticity component that comes out from the Runge-Kutta method and $f_2(x)$ is a ramp function that goes smoothly from $f_2(x_3) = 1$ to $f_2(x_4) = 0$.

The implemented function was:

$$f_2(x) = f(\varepsilon) = 1 - 6\varepsilon^5 + 15\varepsilon^4 - 10\varepsilon^3, \tag{31}$$

where:

$$\varepsilon = \frac{i - i_3}{i_4 - i_3}, \tag{32}$$

and $i_3 \leq i \leq i_4$. The points i_3 and i_4 correspond to x_3 and x_4 positions in streamwise direction respectively. This function is illustrated in Fig.(4).

To ensure good results of a simulation, it's recommended that the distance between x_3 and x_4 correspond to two TS-wavelenghtes and that between x_4 and the end of the domain (x_{max}) correspond to one TS wavelenght.

Numerical Method:

The Eq. (17) to (22) were solved numerically by the schemes described bellow.

The solution was marched in time according to the following steps:

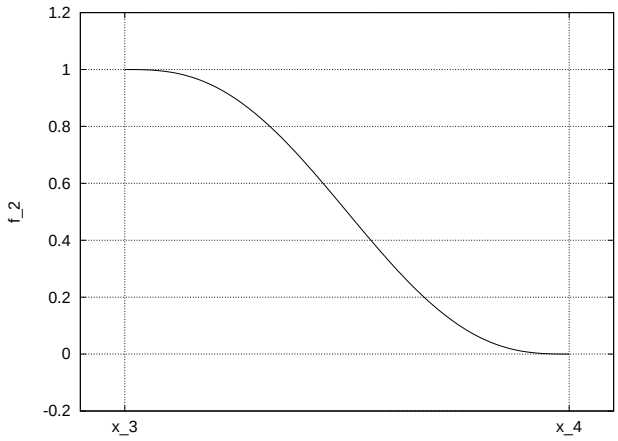

Figure 4: Function used in the damping zone

1. Impose initial conditions using 2D solution for U_{x_k}, U_{y_k} and Ω_{z_k} and set other variables U_{z_k}, Ω_{x_k} and Ω_{y_k} to zero;
2. Introduce disturbances at the wall through the disturbance strip;
3. Calculate the new vorticity distribution in the whole field, except at the wall, integrating the vorticity transport equations (17) to (19);
4. Taper the vorticity disturbances components to zero at the relaminarization area;
5. Calculate the wall normal velocity component (U_{y_k}) by solving the Poisson equation (21);
6. Calculate the streamwise velocity component (U_{x_k}) by using the continuity equation (4) for the 2D mode and the Poisson equation (20) for others modes;
7. Calculate the spanwise velocity component (U_{z_k}) by using the Poisson equation (22);
8. Calculate the streamwise vorticity component generation at the wall by solving the Poisson equation (26);
9. Calculate the spanwise vorticity component generation at the wall solving the Poisson equation (27);
10. return to the second step until the desired integration time is reached.

The time derivative in the vorticity transport equations were discretized with a classical 4^{th} order Runge-Kutta integration scheme (Ferziger and Peric, 1997). The steps 4 to 9 were carried out for each step of the Runge-Kutta method.

The spatial derivatives were calculated using a compact differences schemes. This technique is well documented in (Souza et al., 2001). The Poisson equation (21) was solved using a Full Approximation Scheme (FAS) multigrid. A v-cycle working with 4 grids was implemented. The number of cycles used varies according to the desirable convergence criteria. The adopted criteria was that the residue should be less than 1×10^{-9}. The residue R of the v-Poisson equation is:

$$R = -\frac{1}{Re}\frac{\partial^2 U_{y_k}}{\partial x^2} - \frac{\partial^2 U_{y_k}}{\partial y^2} + \beta_k^2 U_{y_k} - \frac{\partial \Omega_{z_k}}{\partial x} + \beta_k \Omega_{x_k}. \tag{33}$$

3. Code Validation

One way to verify and validate a computer code designed for hydrodynamic stability analysis is to use results from linear and weakly non-linear stability theory. In this section, results from the computations are compared against theoretical results for the linear propagation of oblique waves and experimental and numerical results for the non-linear evolution of wave systems composed of a two-dimensional wave and a pair of oblique waves, known as fundamental resonance and subharmonic resonance.

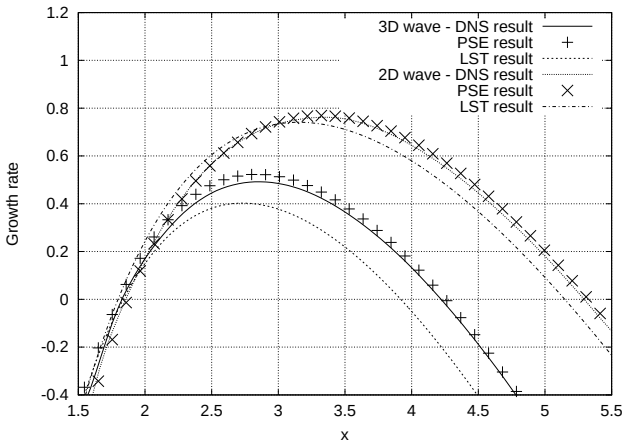

Figure 5: Variation of the amplitude and growth growth rate along the streamwise direction. Comparison between Linear Stability Theory (LST), PSE results and DNS results.

3.1. Linear results

Transition to turbulence may take place in distinct ways, one that is common in a highly disturbed environment known as by-pass transition. Another, when small amplitude disturbances grow linearly at first, reach a non-linear state and then break-down to turbulence. The theory describing the second route is well established, specially for linear and weakly non-linear regimes. In this section the results obtained for the propagation of a oblique wave are compared with linear stability theory and with a weakly non-linear model known as 'Parabolized Stability Equations-PSE' (Mendonça, 2000). Comparisons are presented for the evolution of the disturbance amplitude and growth rate.

A disturbance is followed downstream starting at a position close to the lower branch of the stability diagram ($x/L = 1.5$) until downstream of the upper branch ($x/L = 5.5$). The results are presented in Fig. 5 for a 2D wave and a 3D wave with frequency $\omega_t = f\nu/U_\infty 10$, where f is the dimensional frequency. spanwise wavenumber $\beta = \beta_d L = 20$, where β_d is the dimensional wavenumber. They show that the numerical simulation reproduces the linear theory with a very good accuracy. The differences between the numerical results (both PSE and DNS) and LST results are due to non-parallel effects which are not taken into account in LST.

3.2. Non-linear results

There are many different routes leading to transition due to the non-linear evolution of wave systems. In natural transition a large number of disturbance modes are present, making it difficult to distinguish their isolate effect and very hard to grasp the physics behind it. In order to gain a greater insight into the transition phenomena it is common to study wave system in a more controlled environment. Two classic experiments are well documented and thus represent good tests for numerical simulations. One is the so called fundamental resonance, or K-type resonance, after Klebanoff (Klebanoff et al., 1962), where a two-dimensional wave interacts non-linearly with an otherwise linearly stable pair of three-dimensional waves. The second experiment is a subharmonic resonance problem, or H-type resonance after Herbert (Herbert, 1988; Kachanov and Levchenko, 1984) where a two-dimensional wave destabilizes a linearly stable oblique wave having half the frequency of the 2D wave.

Figures 6 and 7 present the results for fundamental and subharmonic resonance respectively. The numerical results are compared with experimental results and numerical PSE results (Mendonça, 2000). The Fourier modes presented in the figures are label (n, m), where n correspondes to the multiples of the base frequency $n\omega_t$, and m correspondes to the multiples of the spanwise wavenumber $m\beta$. They show that the numerical scheme implemented is able to capture the non-linear resonant amplification of 3D waves (1,1) or (2,1) in the presence of a 2D wave (2,0) for both resonance modes. Figures 8 and 9 show the structure of the streamwise velocity component in a plane parallel to the surface. The characteristic aligned and staggered patterns (Herbert, 1988) for fundamental and subharmonic resonance are clearly shown.

4. A More Complex Non-linear System

When the wave system is composed of both fundamental modes and subharmonic modes, there is a competition between them and the resulting flow pattern depends on the relative amplitude of the 2D wave and the two 3D waves. Other investigations have revealed that the subharmonic resonance is more dangerous than

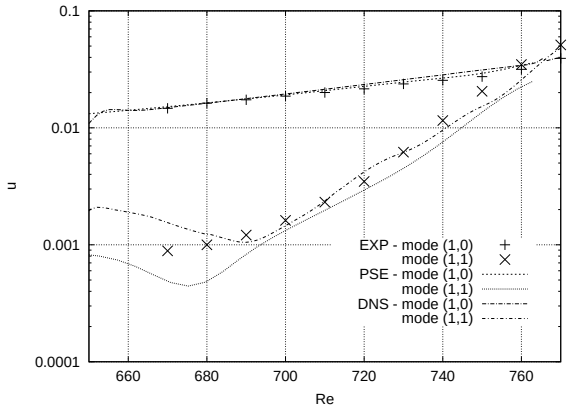

Figure 6: Fundamental resonance. Comparison between experimental (EXP), PSE and DNS results.

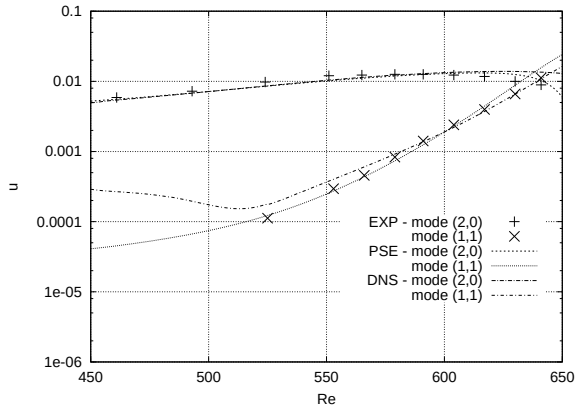

Figure 7: Sub-harmonic resonance. Comparison between experimental (EXP), PSE and DNS results.

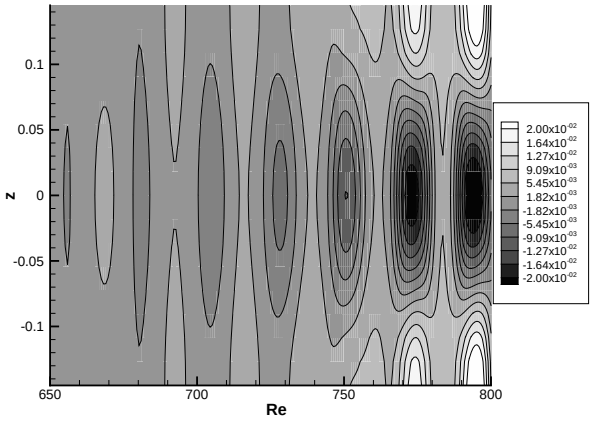

Figure 8: Fundamental resonance. streamwise disturbance velocity contours for y=2.52.

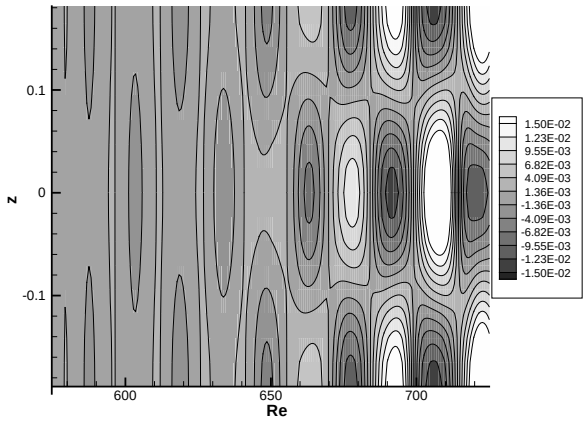

Figure 9: Subharmonic resonance. streamwise disturbance velocity contours for y=2.1504.

fundamental resonance in the sence that much lower initial amplitudes of the 2D wave are enough to trigger the nonlinear mechanism that leads to the excitation of the 3D wave. Also, the subharmonic mode has a larger growth rate than the fundamental mode (Stemmer, 2001; Herbert, 1988).

Recently, Mendonça and Medeiros, 2000 studied wave systems composed of a 2D wave and both fundamental and subharmonic modes using a numerical model based on PSE. The study considered subharmonic and fundamental modes with the same initial amplitude. The conclusions obtained in that study were:

- The subharmonic mode has a stronger growth rate than the fundamental mode and it is destabilized by the 2D wave at lower amplitudes.
- When both modes are present, raising the initial amplitude of the 2D wave has a strong effect on the growth of the fundamental mode, but for the numerical experiments presented in the paper the subharmonic mode is always dominant.
- since the fundamental mode has a higher frequency than the subharmonic mode, in some cases with a low spanwise wavenumber the fundamental mode becomes unstable according to linear stability theory. In this case, due to the resonance, its growth rate is larger than the growth rate of the subharmonic mode.
- Based on the results presented in the paper, subharmonic resonance should be more easily observed.

In the present paper, the study presented by Mendonça and Medeiros, 2000 is extended to include cases where the fundamental and subharmonic waves do not have identical initial amplitudes. Also, the numerical model based on direct numerical simulations allows the study of stronger nonlinear problems, relaxing one of the simplifying assumptions of the PSE weakly nonlinear model.

Out of the total number of numerical experiments performed only two are presented due to space limitations. The first one, presented in Fig. 10 and 11, considers a wave system composed of a 2D wave with frequency

$\omega_t = 3.2$, a fundamental 3D wave with the same frequency and with spanwise wavenumber $\beta = 44$, and a subharmonic wave with half the frequency and with the same spanwise wavenumber. It corresponds to seeding the fundamental mode of Kachanov and Levchenko, 1984 with a subharmonic mode. The initial amplitudes of the 3D modes at the suction and blowing strip are the same, but the two modes have different receptivity characteristics and after a transient region the amplitudes of the resulting eigenmodes may be different.

The results show that, for the relative amplitudes of the 2D wave and the two 3D waves, the fundamental mode has a stronger growth rate and attain a much larger amplitude than the subharmonic mode. As expected the flow field has a structure corresponding to a fundamental resonance. Further experiments indicate that for the present test case, the subharmonic has not yet concluded the transient region at $Re = 650$. In other words, the subharmonic mode is effectively established at around $Re = 700$ at a much lower amplitude when compared with the fundamental mode. In this case, due to the receptivity characteristics of the subharmonic and fundamental modes the breakdown corresponds to that of a fundamental resonance.

According to Herbert, 1988, despite the fact that the subharmonic mode is more dangerous than the fundamental mode, there are certain conditions for which the flow patter leading to breakdown to turbulence corresponds to a fundamental resonance, even when there are also subharmonic modes in the wave system. The results presented by Mendonça and Medeiros, 2000 could not detect this behavior. By simply raising the amplitude of the 2D wave in order to get a stronger resonance with the fundamental mode, it was not possible to detect this response with the current DNS model either. On the other hand it seems that the fundamental resonance is predominant when the initial amplitude of the subharmonic mode is much lower than the initial amplitude of the fundamental.

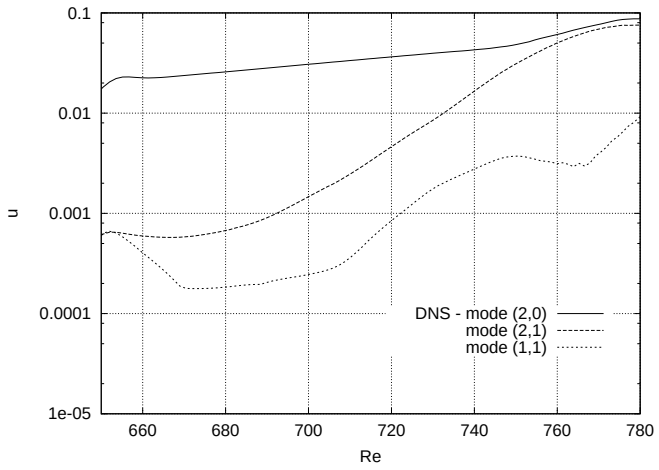

Figure 10: Amplification of the streamwise velocity component due to the nonlinear evolution of a wave system composed of a 2D wave, a fundamental 3D wave and a subharmonic 3D wave.

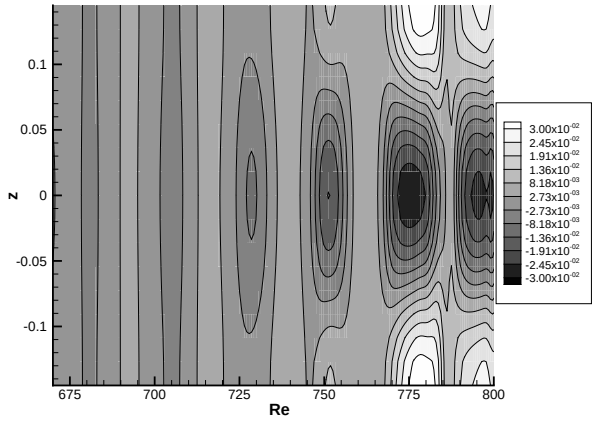

Figure 11: Resulting flow patter. Streamwise disturbance velocity component.

Another experiment was then set up where the initial amplitude of the subharmonic mode is higher than the amplitude of the fundamental mode after the selective filtering in the transient region. The initial condition considered a wave system identical to the experiment of Klebanoff et al., 1962 seeded by a subharmonic wave. In order to delay the resonance between the 2D wave and the fundamental mode, the initial amplitude of the 2D wave was also lower. The results, ilustrated by Figs. 12 and 13, show that the flow field close to breakdown to turbulence corresponds to a subharmonic type resonance.

5. Conclusions

A numerical model based on high order compact differencing schemes to solve the complete Navier-Stokes equations in a direct numerical simulation has been presented. The model has been validated against linear stability theory, nonlinear experimental and PSE numerical results.

The model was used to investigate transition to turbulence when both subharmonic and fundamental resonances are active. The results confirm that the subharmonic mode is the most dangerous since its growth rates are higher and the initial amplitudes necessary to trigger resonance are lower. Nevertheless, it is possible to have transition to turbulence governed by fundamental resonance when the initial amplitude of the subharmonic is lower than the initial amplitude of the fundamental mode.

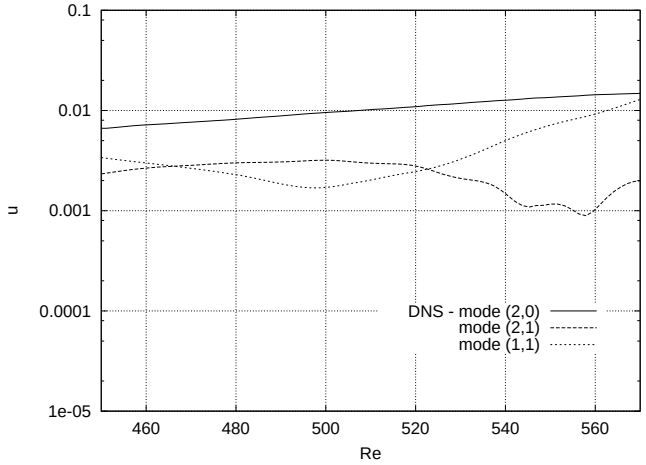

Figure 12: Amplification of the streamwise velocity component due to the nonlinear evolution of a wave system composed of a 2D wave, a fundamental 3D wave and a subharmonic 3D wave.

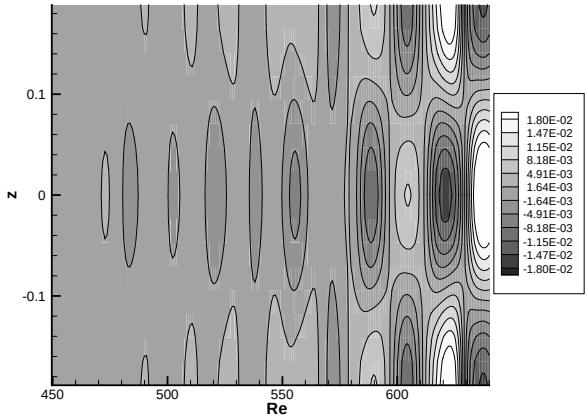

Figure 13: Resulting flow patter. Streamwise disturbance velocity component.

6. Acknowledgments

The first author acknowledge the transition research group of the Institut fur Aerodynamik and Gasdynamik (IAG) from Universitat Stuttgart, where he spent 6 months as a visiting scientist. The financial support received from FAPESP is also ackowledged.

7. References

Carpenter, M., Singer, B., Vatsa, V., Viken, S., and Yamaleev, N., 2002, The Current Status of Unsteady CFD Approaches for Aerodynamic Flow Control, "AIAA Fluid Dynamics Conference", St. Louis, USA.

Fasel, H., 1976, Investigation of Stability of Boundary Layers by a finite-difference model of the Navier-Stokes Equations, "J. Fluid Mechanics", Vol. **78**, pp. 355–383.

Fasel, H. F., Rist, U., and Konzelmann, U., 1990, Numerical Investigation of the Three-Dimensional Development in Boundary Layer Transition, "AIAA Journal", Vol. 28, No. 1, pp. 29–37.

Ferziger, J. H. and Peric, M., 1997, "Computational Methods for Fluid Dynamics", Springer, Springer–Verlag.

Herbert, T., 1988, Secondary instability of boundary-layers, "Ann. Rev. Fluid Mech.", Vol. **20**, pp. 487–526.

Herbert, T., 1991, Exploring Transition by Computer, "Appl. Num. Math.", Vol. **7**, pp. 3–25.

Kachanov, Y. S. and Levchenko, V. Y., 1984, The resonant interaction of disturbances at laminar-turbulent transition in a boundary layer, "J. Fluid Mech.", Vol. 138, pp. 209–247.

Klebanoff, P. S., Tidstrom, K. D., and Sargent, L. M., 1962, The three-dimensional nature of boundary layer instability, "J. Fluid Mech.", Vol. 12, pp. 1–34.

Kloker, M., Konzelmann, U., and Fasel, H., 1993, Outflow Boundary Conditions for Spatial Navier-Stokes Simulation of Transition Boundary Layer, "AIAA Journal", Vol. 31, No. 4, pp. 620–628.

Kloker, M. J., 1998, A Robust High-Resolution Split-Type Compact FD Scheme for Spatial Direct Numerical Simulation of Boundary Layer Transition, "Applied Scientific Research", Vol. **59**, pp. 353–377.

Laurien, E. and Kleiser, L., 1989, Numerical Simulation of Boundary-Layer Transition and Transition Control, "J. Fluid Mechanics", Vol. **199**, pp. 403–440.

Lele, S., 1992, Compact Finite Difference Schemes with Spectral-like Resolution, "J. Computational Physics", Vol. **103**, pp. 16–42.

Meitz, H. L. and Fasel, H. F., 2000, A compact-difference scheme for the Navier-Stokes equations in vorticity-velocity formulation., "J. Comp. Phys.", Vol. **157**, pp. 371–403.

Mendonça, M. T., 2000, Parabolized Stability Equations: A Review, "National Congress of Mechanical Engineering - CONEM 2000", Natal - RN.

Mendonça, M. T. and Medeiros, M. A. F., 2000, On Subharmonic and Fundamental Instability Modes in Boundary Layers, "8th Brazilian Congress of Engineering and Thermal Sciences - ENCIT 2000", Porto Alegre - RS.

Moin, P. and Mahesh, K., 1998, Direct Numerical Simulation: A Tool in Turbulence Research, "Ann. Rev. Fluid Mech.", Vol. **30**, pp. 539–578.

Rai, M. M. and Moin, P., 1989, Direct Simulation of Turbulent Flow Using Finite-Difference Schemes, "27th

AIAA Aerospace Sciences Meeting and Exhibit", Reno, NV.

Souza, L. F., Mendonça, M. T., and Medeiros, M. A. F., 2001, A high resolution Navier Stokes solver for hydrodynamic stability analysis, "22nd CILAMCE, Iberian Latin-American Congress on Computational Methods in Engineering", Campinas - SP.

Stemmer, C., 2001, "Direct Numerical Simulation of Harmonic Point Source Disturbances in an Airfoil Boundary Layer With Adverse Pressure Gradient", PhD thesis, University of Stuttgart.

Wray, A. and Hussaini, M. Y., 1994, Highly Accurate Compact Methods and Boundary Conditions, "Proc. Royal Soc. London", Vol. **A 392**, pp. 373–389.

Zhang, H. and Fasel, H., 1999, Spatial Direct Numerical Simulation of Görtler Vortices, "AIAA Fluid Dynamics Conference", Norfolk, USA.